

Effect of Suspension Plasma-Sprayed YSZ Columnar Microstructure and Bond Coat Surface Preparation on Thermal Barrier Coating Properties

Benjamin Bernard¹ · Aurélie Quet² · Luc Bianchi³ · Vincent Schick⁴ · Aurélien Joulia³ · André Malié⁵ · Benjamin Rémy⁴

Submitted: 8 February 2017 / in revised form: 25 April 2017 / Published online: 19 June 2017
© ASM International 2017

Abstract Suspension plasma spraying (SPS) is identified as promising for the enhancement of thermal barrier coating (TBC) systems used in gas turbines. Particularly, the emerging columnar microstructure enabled by the SPS process is likely to bring about an interesting TBC lifetime. At the same time, the SPS process opens the way to a decrease in thermal conductivity, one of the main issues for the next generation of gas turbines, compared to the state-of-the-art deposition technique, so-called electron beam

physical vapor deposition (EB-PVD). In this paper, yttria-stabilized zirconia (YSZ) coatings presenting columnar structures, performed using both SPS and EB-PVD processes, were studied. Depending on the columnar microstructure readily adaptable in the SPS process, low thermal conductivities can be obtained. At 1100 °C, a decrease from 1.3 W m⁻¹ K⁻¹ for EB-PVD YSZ coatings to about 0.7 W m⁻¹ K⁻¹ for SPS coatings was shown. The higher content of porosity in the case of SPS coatings increases the thermal resistance through the thickness and decreases thermal conductivity. The lifetime of SPS YSZ coatings was studied by isothermal cyclic tests, showing equivalent or even higher performances compared to EB-PVD ones. Tests were performed using classical bond coats used for EB-PVD TBC coatings. Thermal cyclic fatigue performance of the best SPS coating reached 1000 cycles to failure on AM1 substrates with a β-(Ni,Pt)Al bond coat. Tests were also performed on AM1 substrates with a Pt-diffused γ-Ni/γ'-Ni₃Al bond coat for which more than 2000 cycles to failure were observed for columnar SPS YSZ coatings. The high thermal compliance offered by both the columnar structure and the porosity allowed the reaching of a high lifetime, promising for a TBC application.

✉ Luc Bianchi
luc.bianchi@safrangroup.com

Benjamin Bernard
benjamin.bernard@safrangroup.com

Aurélie Quet
aurelie.quet@cea.fr

Vincent Schick
vincent.schick@univ-lorraine.fr

Aurélien Joulia
aurelien.joulia@safrangroup.com

André Malié
andre.malie@safrangroup.com

Benjamin Rémy
benjamin.remy@univ-lorraine.fr

- ¹ Safran Tech, Plateforme Aubes de Turbines Avancées, 171 Boulevard de Valmy, 92700 Colombes, France
- ² CEA-DAM, Le Ripault, BP 16, 37260 Monts, France
- ³ Safran Tech, Pôle Matériaux et Procédés, Rue de Jeunes Bois, Châteaufort, CS 80112, 78772 Magny-les-Hameaux, France
- ⁴ LEMTA Université de Lorraine, 2 Avenue de la forêt de Haye, BP 160, 54504 Vandoeuvre-lès-Nancy, France
- ⁵ Safran Aircraft Engines, Rue Maryse Bastié, BP 129, 86101 Châtellerault, France

Keywords columnar structure · lifetime · suspension plasma spraying · thermal barrier coating · thermal conductivity · YSZ

Introduction

Over many years, thermal barrier coatings (TBCs) were studied in order to improve gas turbine efficiency. The increase in the thermal insulation performances of the ceramic top layer of TBCs, mainly composed of yttria-

stabilized zirconia (YSZ), was identified as a main issue in the increase in the operating temperatures of the next generation of turbine engines (Ref 1). Since the 1980s, the most efficient deposition process regarding operating conditions of high-pressure parts (mainly thermal cyclic resistance) is electron beam physical vapor deposition (EB-PVD). A high-energy electron beam is used to vaporize an ingot of YSZ. Then, vapors are condensed on the surface of the metallic substrate leading to the coating. A highly thermal-compliant columnar structure is then obtained, allowing a high lifetime. But this microstructure also induces strong heat flux paths between columns which limits the ability to design low-thermal-conductivity coatings using EB-PVD (Ref 1–3). On the other hand, atmospheric plasma spraying (APS), widely used before the 1980s, consists of injecting powder through a plasma jet in order to be melted and accelerated (Ref 4). Then, molten particles are spread onto a metallic substrate as individual splats which are stacked to form a lamellar microstructure. This typical microstructure is favorable to low thermal conductivity. It is also very sensitive to a thermal expansion mismatch, between the ceramic and metallic part of the TBC, leading to a relatively low lifetime on the high-pressure components of the turbine engine, like mobile blades, also considered as a main issue (Ref 5, 6). However, this kind of coating is successfully and commonly applied on combustion chamber, which is not exposed to similar thermal mismatch (Ref 7).

Efforts have been made in order to propose new ceramic compositions to decrease thermal conductivity. Some materials appeared promising, such as rare earth zirconates, complex perovskites, lanthanum aluminates, which present a lower bulk thermal conductivity compared to YSZ (Ref 8–12). Nevertheless, the lifetime performance of these new compositions is lower than YSZ coatings mainly due to lower mechanical properties such as the lower toughness of zirconates for example (Ref 10, 13).

Many studies have been carried out on processes in order to provide an YSZ top coat with improved performance. Using nano-agglomerated powder through a plasma jet, bimodal microstructures were reached (Ref 14). In that case, un-melted or partially melted nanoparticles were embedded in a typical lamellar plasma-sprayed microstructure, allowing a decrease in thermal conductivity and an increase in sintering resistance (Ref 15, 16). However, the lamellar structure seemed unpromising for lifetime resistance. Sol-gel process was also studied leading to highly porous and highly insulative YSZ layers (Ref 17). Moreover, reinforced sol-gel layer has demonstrated a lifetime comparable to YSZ EB-PVD coatings (Ref 18). Highly thermal-compliant structures were also reached by plasma spray physical vapor deposition (PS-PVD) and were identified as promising for TBCs enhancement

(Ref 19, 20). In that case, powders were injected through a high-energy plasma jet in a low vacuum spray booth. Particles were vaporized by the high-energy plasma and then condensed on the substrate. The ability of PS-PVD to coat complex parts such as turbine blades was also demonstrated (Ref 19).

From the 2000s, the use of liquid mediums, to carry nanoparticles, has been developed in order to promote nanostructured coatings via plasma spraying. The use of a liquid medium was proposed in order to overcome limitations on the size of particles ($>5\ \mu\text{m}$) injected through a plasma jet in an APS process using a carrier gas medium (Ref 21). Thus, nanosized particles in suspension, or ceramic precursors in solution, were injected through a plasma jet resulting in suspension plasma spraying (SPS) and solution precursor plasma spraying (SPPS), respectively (Ref 22). These processes allowed production of coatings with a multiscaled porosity covering 4 orders of magnitude which was promising for the enhancement of thermal insulation properties (Ref 23). Moreover, different microstructures were obtained using SPS or SPPS such as homogenous structures, vertically cracked structures and more particularly columnar structures which were unusual for thermal sprayed coatings (Ref 22–28). In the case of columnar structures, the low size of particles ($<5\ \mu\text{m}$) used for SPS process, allowed them to be deviated by the plasma flow in the vicinity of the substrate (Ref 29). It led to a combined normal and lateral growth of columns around the substrate asperities assumed to be the explanation of these typical cone shape columns (Ref 30). Figure 1 is a schematization of the coating buildup, inspired by the study of Van Every et al. (Ref 30), which explains the formation of SPS columnar structures. The cone shape results from the combination of the normal impingement of big un-deviated particles and the lateral impingement of small strongly deviated particles. Some studies show that relevant parameters linked to SPS process such as substrate roughness, particle size or the suspension load, allow control of the shape, size and organization of SPS columns (Ref 31–33).

The literature also reports a better thermal cycling resistance than YSZ APS coatings due to the columnar shape of these SPS coatings allowing thermal compliance of the top coat (Ref 32, 34–36). YSZ porous columnar structures also led to a significant decrease in thermal conductivity in the range of $0.6\text{--}1\ \text{W m}^{-1}\ \text{K}^{-1}$ compared to typical values of YSZ EB-PVD coatings ($\sim 1.5\ \text{W m}^{-1}\ \text{K}^{-1}$) (Ref 34, 37, 38). As for PS-PVD, columnar suspension plasma-sprayed coatings were applied to turbine blade parts successfully (Ref 39).

The aim of this study is to present and analyze the thermal insulation and lifetime properties of different YSZ columnar structures performed using SPS. Particularly, it is

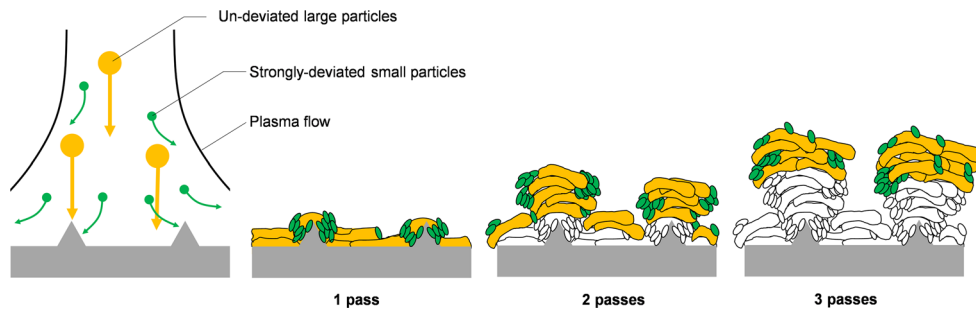


Fig. 1 Coating buildup of SPS columnar structure

shown that columnar structures produced by SPS are able to equalize, and in some cases surpass, the lifetime of YSZ EB-PVD depending on the compaction of the columns and bond coat preparation. The ability of the SPS process to perform such columnar coatings on real turbine parts is also investigated.

Experimental Procedure

Spraying Setup and Conditions

An YSZ ethanol-based suspension, with 7 wt.% Y_2O_3 and medium particle diameters around $0.5 \mu m$, were purchased from Treibacher Industrie AG. Suspensions were stored in a pressurized vessel and maintained with magnetic stirring during the deposition step. The suspension was injected radially through the plasma jet. A F4-VB type plasma torch (6-mm-internal-diameter nozzle) from Oerlikon-Metco™ was used to perform YSZ coatings. Coatings were achieved in a ventilated spray booth maintained at atmospheric pressure. The standoff distance was fixed at 50 mm. The substrate cooling was ensured by compressed air jets and liquid CO_2 jets. Cooling jets were oriented in order to avoid perturbation during coating. Two spraying conditions were used and are described in Table 1.

Coatings were deposited onto Hastelloy X substrates with an aluminized NiAl bond coat for thermal conductivity measurements and microstructural investigations. In

that case, the bond coat was performed using the Snecma vapor aluminizing process (APVS). In order to improve adhesion of the YSZ layer by a thin thermally grown oxide (TGO) layer of Al_2O_3 , the bond coat was preheated at $1100 \text{ }^\circ C$ for 1 h. For thermal cyclic fatigue tests, an AM1 superalloy with two different bond coats (β -(Ni,Pt)Al and platinum-diffused γ -Ni/ γ' -Ni₃Al) was used. First of all, electroplating of Pt was carried out on AM1 substrate. Heat treatment after the electroplating step allowed to provide a γ -Ni/ γ' -Ni₃Al bond coat. An additional APVS step allowed to carry out a β -(Ni,Pt)Al bond coat. A preheating step at $1100 \text{ }^\circ C$ of 1 h was applied to some samples and will be detailed later. Roughness of substrate was managed using sandblasting with corundum of two sizes: 79 and $350 \mu m$. The microstructures were observed via scanning electron microscopy (SEM) on a Leo 435VPi microscope.

For comparison of the insulation and lifetime performance, SPS coatings were compared with YSZ EB-PVD coatings. These coatings were provided by Safran Aircraft Engines and were representative of coatings performed on current engines.

Thermal Conductivity Calculation

Thermal conductivity value was calculated using Eq 1 where λ is the thermal conductivity, α is the thermal diffusivity, ρ the coating density and C_p the heat capacity. The values of α , ρ and the C_p of the coating were measured separately.

$$\lambda = \alpha \rho C_p \tag{Eq 1}$$

Image analysis was chosen in order to characterize coating density. SEM cross sections were recorded on the Leo 435VPi microscope. Then, using ImageJ software, SEM pictures were converted into binary images for porosity measurements. The value of the coating density ρ_c was calculated using Eq 2 where P is the porosity and ρ_{YSZ} the theoretical value of bulk YSZ. The relative error on porosity was estimated to be $\pm 5\%$ of the measured value of porosity.

Table 1 Spraying conditions

	Condition	
	1	2
Mixture Ar/He/H ₂	47%/47%/6%	50%/50%
Power	32.2 kW	22.4 kW
Enthalpy	$2.2 \times 10^7 \text{ J/kg}$	$1.5 \times 10^7 \text{ J/kg}$
Suspension feed rate	25 g/min	44 g/min

$$\rho_c = \rho_{\text{YSZ}}(1 - P) \quad (\text{Eq 2})$$

Differential scanning calorimetry (DSC) was carried out for measurement of the specific heat capacity C_p of the substrate and the SPS coating. The DSC device used in the study was a 96 LineEvo from Setaram. Powders obtained from a delaminated YSZ coating were used for the DSC analysis.

Thermal diffusivity was obtained using a flash method and numerical estimation. Here, the sample (a bilayer substrate + YSZ coating) was illuminated by a laser flash inducing a rise in temperature (thermogram) characteristic of the thermal properties of the system. In order to reach thermal diffusivity values of the coating from flash experiments, the heat Eq 3 where φ , T and S represent the heat flux, the temperature (T) and the illuminated surface, respectively, was solved in Laplace space using a quadrupole method as widely described in a previous study (Ref 38).

$$\varphi(t) = -\lambda S \frac{dT(t)}{dt} \quad (\text{Eq 3})$$

A simulated thermogram was obtained in Laplace space. By using a de Hoog algorithm (Ref 40), a numerical inversion was carried out in order to obtain a numerical thermogram in time. The estimation of the thermal diffusivity of the coating was allowed by a least square fitting between the experiment and the simulated thermogram using a Levenberg-Marquardt algorithm (Ref 41, 42). The least square fitting was done by adjusting the values of α and ρC_p of the coating. The substrate thermal properties were supposed to be known and required preliminary flash experiment on the substrate alone. As described in literature, the numerical estimation was mostly sensitive to the thermal diffusivity and not to C_p and ρ which were reached using DSC and image analysis here (Ref 43).

In order to perform flash measurement, a high-temperature experimental bench developed by the LEMTA laboratory at Lorraine University (France) was used. Square samples (40 mm × 40 mm) were placed in a tubular furnace made from Carbolite® and heated from room temperature up to 1100 °C. The thickness was about 1.5 mm including 300 μm of YSZ coating. All the coating thicknesses were measured by image analysis on cross sections. The flash was generated using a Neodymium glass laser with a wavelength of 1053 nm from the Quantel Company. The thermograms were recorded using an infrared camera InSb Cedip® Titanium SC7000 with a [1.5–5.5 μm] band. Due to its semitransparency, the ceramic layer induced perturbations of the thermogram recorded by IR camera (Ref 44, 45). In order to overcome the semitransparency of

YSZ, a thin layer of graphite (about 10–20 μm) was applied on the surface of YSZ coatings.

Isothermal Cyclic Tests

The lifetime of YSZ coatings was assessed via thermo-cyclic fatigue (TCF) tests. The test consisted of an isothermal cyclic test performed in a furnace, where samples were heated at 1100 °C for 15 min. The temperature was maintained at 1100 °C for a further 45 min before rapid compressed air cooling. Cooling ensured a temperature of the tested samples less than 80 °C after 15 min. The failure criterion was fixed at 20% of spallation of the coating surface.

Results and Discussion

Microstructural Features

Columnar structures, shown in Fig. 2, were obtained using the spraying conditions in Table 1. The first one presents typical features for SPS columnar structures with columns separated by inter-columnar voids (Fig. 2a). Columns present a typical cauliflower shape on the SEM top surface view (Fig. 2b). This results from a combination of lateral and normal coating growth velocities. They are provided by the difference of trajectories experienced by particles in the vicinity of the substrate, where the plasma flow is strongly deviated (Ref 30). The inter-columnar voids were optimized in order to keep a well-defined columnar structure with a high cauliflower-like compaction level. Here, the use of a high torch linear speed (1.5 m/s) results in a low thickness of deposited material with each pass of the torch before the substrate (0.7 μm/pass). Thus, a longer duration was allowed for the column organization allowing reduction in the inter-columnar voids (Ref 33). A schematization of the mechanism is shown in Fig. 3. The coating density (reached by image analysis on cross sections) of the coating performed using spraying Condition 1 was measured at 4515 kg/m³.

The coating, performed using spraying Condition 2 of Table 1, has a singular microstructure with columns (see cauliflowers in Fig. 2d), but for which the inter-columnar voids tend to disappear (Fig. 2c). The microstructure was called a compact columnar structure. The compact shape results from the greater thickness deposited by each pass of the torch (1.32 μm/pass) due to the higher suspension feed rate used (see Table 1). It leads to a rapid overlapping of columns (Ref 33). The coating density of the coating (reached by image analysis on cross sections) performed using spraying Condition 2 was measured at 4880 kg/m³.

Fig. 2 SEM cross section and surface pictures of SPS coatings obtained using condition 1 (a, b) and 2 (c, d) of Table 1

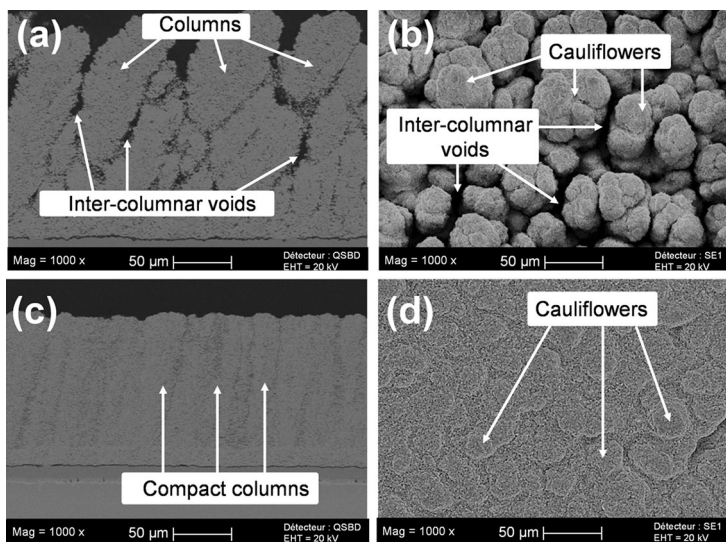
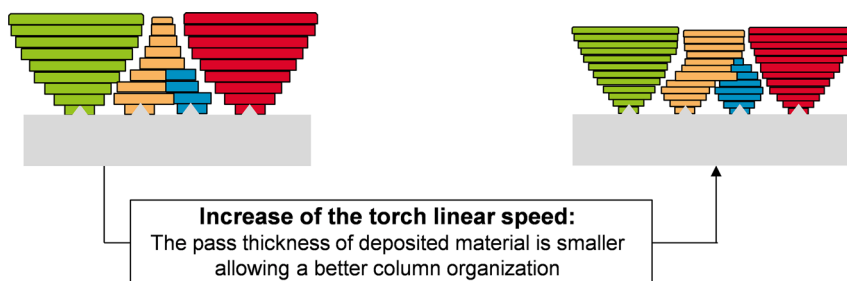


Fig. 3 SPS mechanism buildup allowing a decrease in inter-columnar voids in SPS columnar structures



Thermal Insulation Properties

Optimized columnar microstructure 1 and 2, named SPS columnar and SPS compact columnar microstructures, respectively, were characterized to reach thermal conductivity at high temperature using the flash method and DSC. An EB-PVD coating provided by Safran Aircraft Engines and representative of a hot section part TBC coating from current gas turbine engines was also characterized. Results were recorded from 25 °C up to 1100 °C. Characterization was not performed beyond 1100 °C in order to preserve the integrity of the NiAl-Hastelloy X substrate. The evolution of thermal conductivity with respect to temperature is plotted in Fig. 4 for the three samples characterized: a SPS columnar coating, a SPS compact columnar coating and a columnar EB-PVD coating.

Measurement at 25 °C of the thermal conductivity was consistent with values obtained using another experimental flash method bench and similar YSZ coatings (Ref 38). EB-PVD shows a lower thermal insulation power at 25 °C with a thermal conductivity of 1.58 W m⁻¹ K⁻¹ compared to 0.8 W m⁻¹ K⁻¹ for the SPS columnar structure and 0.71 W m⁻¹ K⁻¹ for the SPS compact columnar structure.

For both SPS coatings, the thermal conductivities present an almost flat profile over the tested temperature range. The EB-PVD thermal conductivity seems to slightly decrease with an increase in temperature. This could be attributed to the increase in anharmonic interaction between phonons at high temperature.

In the end, the thermal conductivities at high temperature of SPS coatings are lower than EB-PVD with a value of 0.86 and 0.70 W m⁻¹ K⁻¹ at 1100 °C for the SPS columnar structure and the SPS compact columnar structure, respectively. Results could be mainly attributed to the difference of porosity volume and distribution through SPS- and EB-PVD-specific microstructures.

First of all, inter-columnar voids are observed for both columnar structures reached by SPS (coating performed using spraying Condition 1 of Table 1) and EB-PVD. This specific porosity, due to its elongated shape, can increase radiation contribution to thermal conductivity. However, the main difference between the two coatings remains the intra-columnar porosity. Coating achieved by SPS process is known to present a high and well-dispersed porosity volume (Ref 23, 38). On the contrary, for EB-PVD columns, the porosity is mainly located in the fringe of

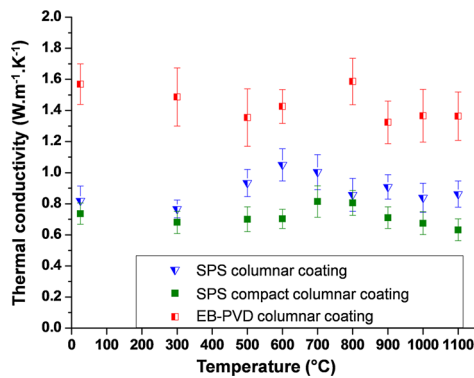


Fig. 4 Resulting thermal conductivity measurements

columns for which the inner part is rather dense (Ref 38). As a consequence, the SPS columnar structure presents a higher thermal resistance toward the columns compared to EB-PVD coatings. SPS columnar coatings roughly present the same intra-columnar porosity volume irrespective of the studied microstructure: the well-defined columnar structure or the compact columnar structure (respectively, spraying Conditions 1 and 2 from Table 1). However, for the compact columnar structure, the inter-columnar porosity is almost totally suppressed (see Fig. 2). By the way, the radiation contribution is reduced leading to a slightly lower thermal conductivity. These heat transfer mechanisms are summarized in Fig. 5 for a well-defined microstructure reach by SPS and a typical EB-PVD coating.

In this study, we have measured thermal conductivity values in the range of $0.6\text{--}1\text{ W m}^{-1}\text{ K}^{-1}$ (from room temperature to $1100\text{ }^{\circ}\text{C}$). These values are promising for future TBC applications and are quite similar to those obtain in literature for YSZ SPS coatings (Ref 34, 37).

Isothermal Cyclic Tests

The lifetime of YSZ coatings was assessed using an isothermal cyclic test in a furnace at $1100\text{ }^{\circ}\text{C}$. The resulting lifetimes for the two optimized SPS columnar structures are shown in Fig. 6. An AM1 substrate was used with two different bond coats, $\beta\text{-(Ni,Pt)Al}$ and platinum-diffused $\gamma\text{-Ni}/\gamma'\text{-Ni}_3\text{Al}$ (Pt- γ/γ'), which are usually used for YSZ EB-PVD coatings. Two levels of roughness were analyzed. Bond coat roughness was identified as a key parameter in order to modulate the size of SPS columns and their organization (Ref 32, 33). It is widely assumed that a preheating step, before the deposition of the top coat, enhances the lifetime of TBCs composed of an YSZ top coat obtained by EB-PVD and an aluminized bond coat (Ref 46). Therefore, a preheating step was performed at $1100\text{ }^{\circ}\text{C}$ for 1 h for both bond coats.

Effect of the SPS Microstructure on Lifetime

With regards to Fig. 6, almost all SPS coatings reach 500 cycles to failure which is representative of the lifetime reported in literature for similar YSZ coatings (Ref 24, 34, 35, 37). In the present study, EB-PVD coatings reach 1000 cycles to failure on AM1 with a $\beta\text{-(Ni,Pt)Al}$ bond coat. No samples of YSZ EB-PVD coating were tested on platinum-diffused $\gamma\text{-Ni}/\gamma'\text{-Ni}_3\text{Al}$ (Pt- γ/γ'). In the literature, YSZ EB-PVD coatings, including an AM1 substrate with a Pt- $\gamma\text{-Ni}/\gamma'\text{-Ni}_3\text{Al}$ bond coat performed using a spark plasma sintering process, were tested using similar TCF conditions and reached 1800 cycles to failure (Ref 47). With regards to the performance of SPS coatings, columnar structures appeared to be more resistant to TCF test. They resist up to 1000 cycles to failure on AM1 with $\beta\text{-(Ni,Pt)Al}$ and to 2145 cycles to failure on AM1 substrate with a Pt- γ/γ' bond coat. Even if an SPS compact columnar structure presents lower lifetime resistance than an SPS columnar one, results are promising on AM1 with a Pt- γ/γ' bond coat. In that case, TCF tests shows 1300 cycles to failure for SPS compact columnar structures.

Microstructures of SPS coatings are shown in Fig. 7 after a TCF test. Irrespective of the columnar structure (compact or not), cracks appeared after cycling. It is commonly admitted that vertical cracks, as well as columnar structure, are able to bring thermal compliance to the top coat allowing a higher thermal cycling resistance. A recent study using an ICP (in situ coating properties) sensor was performed on homogeneous, vertically cracked and columnar structure coated by SPS and showed that the best thermal compliance was reached by the columnar structure (Ref 36). However, homogenous structure presented a lower thermal compliance compared to vertically cracked structures. The in situ segmentation that occurs in our SPS columnar structures probably extent the lifetime compared to the initial un-segmented state of the coating.

In an SPS columnar structure, a high thermal compliance probably comparable to EB-PVD is allowed by the morphology of the columns at the beginning of the TCF test ($t_{0,\text{col}}$). During thermal cycling, the microstructure evolves and is probably submitted to a sintering effect leading to a more rigid coating and a loss of strain tolerance. The typical shape of SPS columnar structures with shadowed columns and a quite homogenous initiation zone at the base of columns are segmented during the test ($t_{\text{cracks,col}}$). Generated cracks enhance thermal compliance and allow the coating to resist to several additional cycles of TCF tests. In the end, the YSZ coating is suddenly debonded from the bond coat and fails ($t_{\text{fail,col}}$). For the SPS compact columnar structure, the initial microstructure is not really able to accommodate thermal mismatch ($t_{0,\text{col/comp}}$) between substrate and top coat. Early, large cracks probably appear between compact

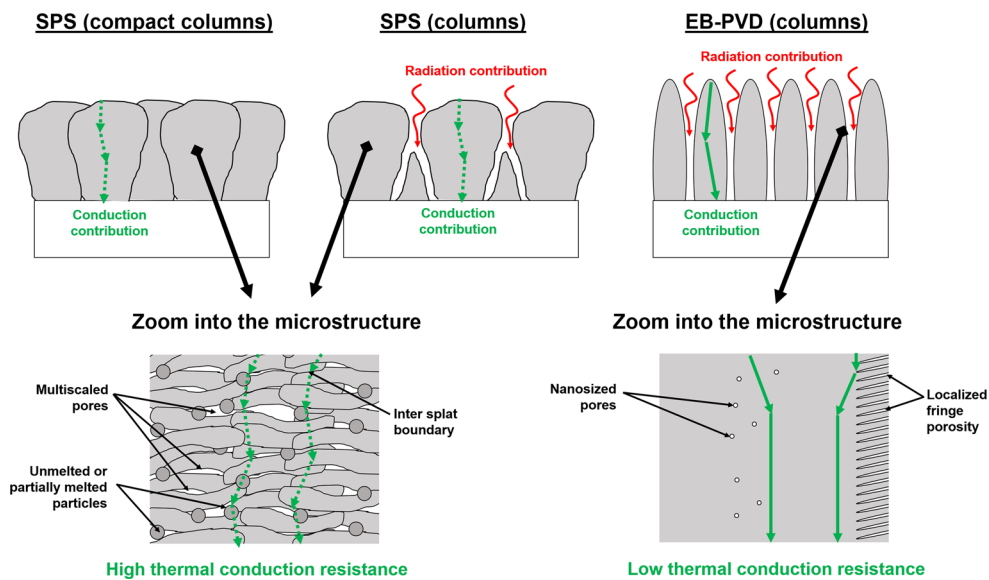
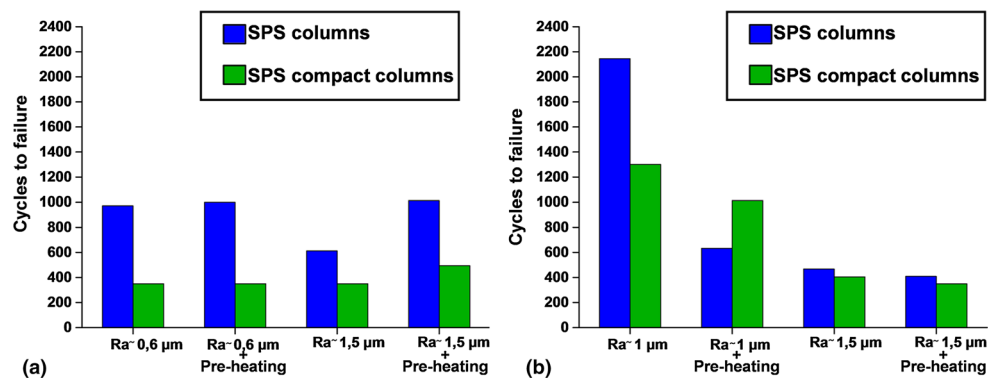


Fig. 5 Schematization of heat diffusion through the two SPS columnar structures and an EB-PVD coating proposed to explain thermal conductivity values

Fig. 6 Thermal cyclic fatigue resistance of YSZ SPS columnar structure and YSZ SPS compact columnar structure coated on AM1 with a β -(Ni,Pt)Al bond coat (a) and a Pt- γ/γ' bond coat (b). Dispersion is measured at ± 200 cycles to failure



columns ($t_{\text{cracks,col/comp}} < t_{\text{cracks,col}}$) and allow thermal compliance. As well as for the SPS columnar structure, the compact cracked morphology evolved, sintered and leads in the end to a similar failure whereby the top coat is suddenly debonded from the bond coat ($t_{\text{fail,col/comp}} < t_{\text{fail,col}}$). The evolution of morphology and the characteristic time described above are schematized in Fig. 8.

Effect of the Bond Coat on Lifetime

The bond coat composition and surface preparation seem to be the most relevant parameters to enhance lifetime resistance of SPS coatings. The best results for TCF tests are obtained on Pt- γ/γ' irrespective of the morphology of SPS columns (compact or not). This kind of bond coat, developed especially for YSZ EB-PVD top coat, is more resistant to oxidation in comparison with β -(Ni,Pt)Al and could explain the better results on Pt- γ/γ' (Ref 48).

As the preparation process of β -(Ni,Pt)Al and Pt- γ/γ' are different, the second bond coat results in an initial mean roughness Ra of about 1 μm . This roughness is suitable for the formation of SPS columnar coating without any bond coat sand blasting. On the contrary, the β -(Ni,Pt)Al is naturally smoother and needs sand blasting in order to get a columnar structure using SPS (here Ra = 0.6 μm). The ability to perform a SPS coating without sand blasting could be beneficial for the lifetime of the TBC. In fact, no additional strain from blasting is added in this case which also leads to higher performance in the TCF test.

Effect of Bond Coat Mean Roughness on Lifetime

As described in literature, substrate roughness greatly impacts the shape, size and organization of columns performed by SPS (Ref 31-33). Here, two levels of substrate mean roughness Ra were tested for the two different bond coats used. Increasing the mean roughness Ra of the bond

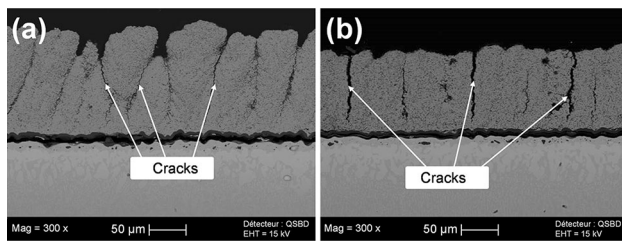


Fig. 7 SEM images of SPS columnar structure (a) and SPS compact columnar structure after TCF test. The substrates used were AM1 with Pt- γ/γ' with a roughness of 1 μm

coats led to an increase in the mean diameter of columns as expected with literature observations (Ref 32, 33). The effect on lifetime is shown in Fig. 9(a) where the evolution of performance during TCF test is expressed in % compared to the reference test. Results took into account only the effects for which a difference of 200 cycles to failure are observed with the reference sample, value corresponding to the dispersion of the results for the TCF test.

Irrespective of the bond coat or SPS YSZ column morphology, a loss of performance was observed when the substrate mean roughness R_a was increased. In fact, an increase in mean roughness has a strong impact on column morphology. Columns are larger and their size is much dispersed (Ref 32, 33). Figure 10 shows two YSZ SPS columnar structures on a β -(Ni,Pt)Al bond coat. The coating, performed on the rougher substrate (here $R_a = 1.5 \mu\text{m}$), presents larger columns. The loss of organization between columns, as well as the increase in column sizes, could induce an inhomogeneity of thermal compliance. This leads to an increase in internal stress at some locations which could speed up debonding of the YSZ SPS top coat.

Effect of the Preheating of Bond Coat on Lifetime

With a similar approach used for the effect of substrate roughness, the effect of a preheating step on bound coated substrates prior SPS top coat deposition on lifetime is shown in Fig. 9(b). For the β -(Ni,Pt)Al bond coat, the lifetime resistance of YSZ SPS columnar structure is increased by about 50% in regard to the initial performance. The preheating step before YSZ EB-PVD deposition is described in literature as an efficient way to improve lifetime of the TBC (Ref 46). In this case, the preheating allowed forming a stable TGO layer composed of α - Al_2O_3 . Rumpling is then attenuated and lifetime resistance increases. A similar behavior could explain the results for TBCs including an YSZ SPS columnar top coat.

Nevertheless, the preheating of the Pt- γ/γ' bond coats appears to be detrimental. In fact, for this kind of bond coat, it is supposed that the formation of a stable α - Al_2O_3 is

not reached with the used preheating cycle. In Pt- γ/γ' bond coats, TGO is formed by the oxidation of the γ' - Ni_3Al . The aluminum content migrated deeper from the AM1 superalloy. In this case, the duration of the preheating (1 h) was probably insufficient to stabilize a α - Al_2O_3 TGO. It was also assumed that some transition oxides, which are detrimental for lifetime resistance, were formed during this preheating stage. However, additional experiments are required to define an improved preheating treatment (probably with a longer duration) for Pt- γ/γ' bond coats.

Failure Mechanisms

Failure was observed near the TGO for all SPS samples tested by TCF tests. Some examples are given in Fig. 11. Irrespective of the structure of SPS coating and bond coat used, failures were mainly driven by a sudden debonding of the top coat with a loss of adhesion in the TGO region (under, or above the TGO and in some cases, inside the TGO with a cohesive failure).

Rumpling was already observed for SPS YSZ coatings performed on NiCoCrAlY bond coats and contributed to failure (Ref 34). These features were also observed in the present study. On the two bond coats used, some examples of rumpling are observed as shown in Fig. 12. The bond coat presents an important deformation, while the YSZ top coat keeps at the interface the shape of the initial state of the substrate. It induces stress which promotes cracks. Rumpling is, however, mainly observed for the β -(Ni,Pt)Al. It is commonly accepted that Pt- γ/γ' presents a higher resistance to this kind of deformation (Ref 48–50). Nevertheless, even if rumpling provides weakness at the interface and generates cracks, the sudden failure by debonding at the interface also suggests an edge delamination similar to an YSZ EB-PVD coating (Ref 51). The critical thickness of TGO allowing adhesion of the TBC system was not carried out in these experiments and will be investigated in a further study. Particularly, the TGO growth will be investigated by analysis of samples for which the TCF test was interrupted at different times before the failure.

Application to Real Components

An YSZ SPS columnar coating was applied to a nozzle guide vane (Fig. 13) and to a blade (Fig. 14) from a high-pressure turbine of a current aero-engine. In both cases, coating is adherent to the component without debonding after spraying.

For the nozzle guide vane, the columnar structure is maintained all along the component profile. Only the convex part of the component was sprayed during the study. On this side, the low variation of angles or standoff distances during spraying allowed keeping a structure

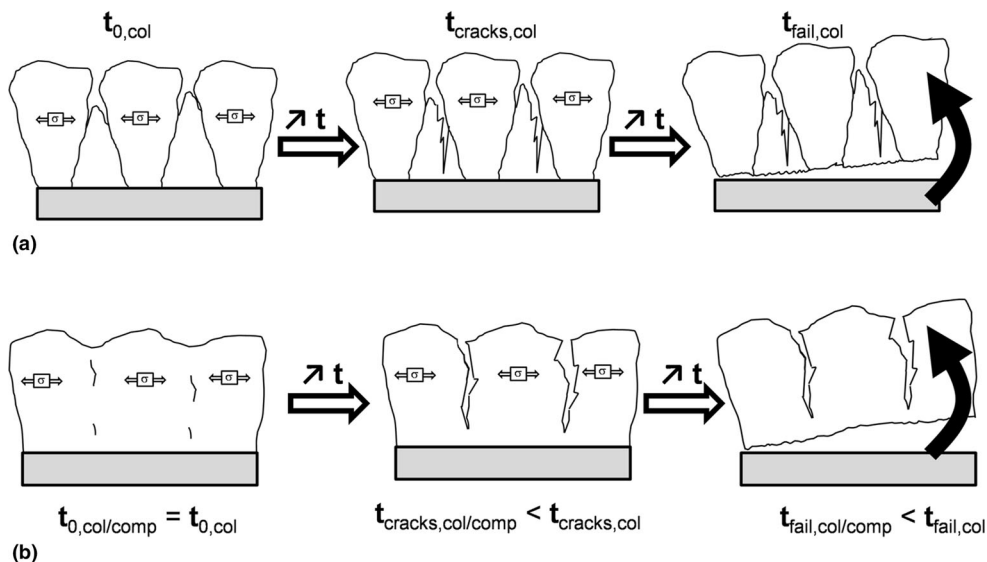


Fig. 8 Microstructural behavior during TCF test for YSZ SPS columnar structure (a) and for YSZ SPS compact columnar structure (b)

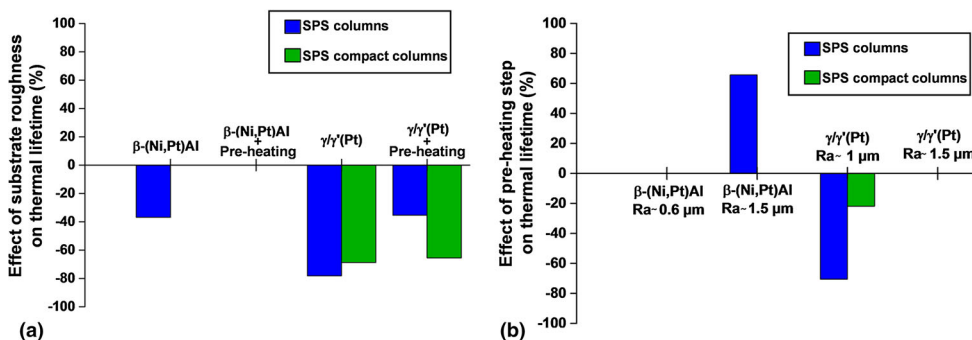


Fig. 9 Effect of substrate roughness (a) and preheating step of bond coat prior to YSZ deposition (b) on TCF performances of SPS coatings

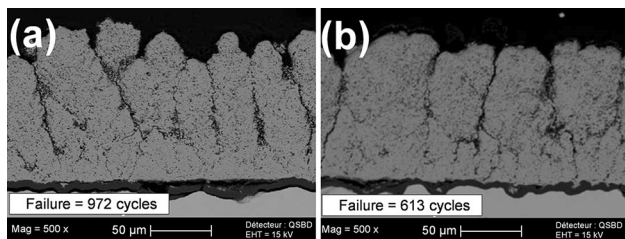
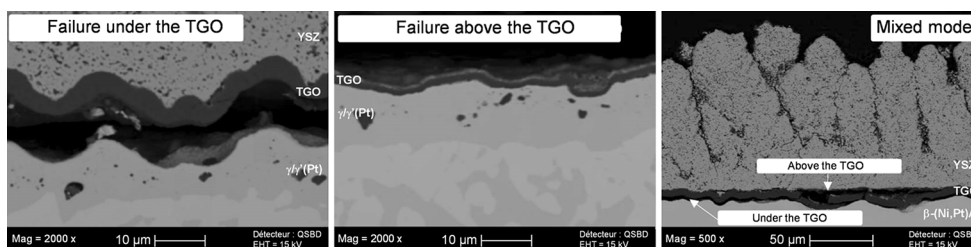


Fig. 10 Evolution of YSZ columnar structure on a substrate roughness of 1 μm (a) and 1.5 μm (b) on a Pt-γ/γ'

which is not drastically perturbed. Only the orientation of the columns is affected and could be attributed to a variation of the deposition angle. The profile of the vane is complex and not flat between regions 1 and 3 shown in Fig. 13. Region 4 shows the connection radius between the vane 1 and the platform. In this location, the spray angle is almost off normal and does not allow a well-defined columnar structure. Coating is composed of cracks and compact columns. The coating thickness needs to be

Fig. 11 Main microstructural failure feature observed after TCF tests



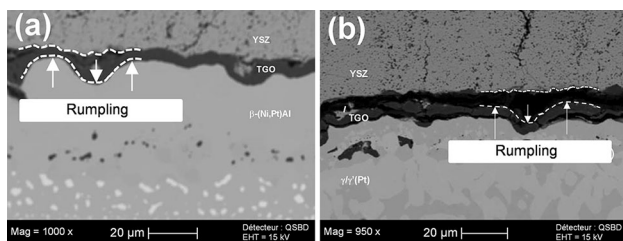


Fig. 12 Observation of rumpling at the interface for the Pt- γ/γ' bond coat (a) and the β -(Ni,Pt)Al bond coat (b)

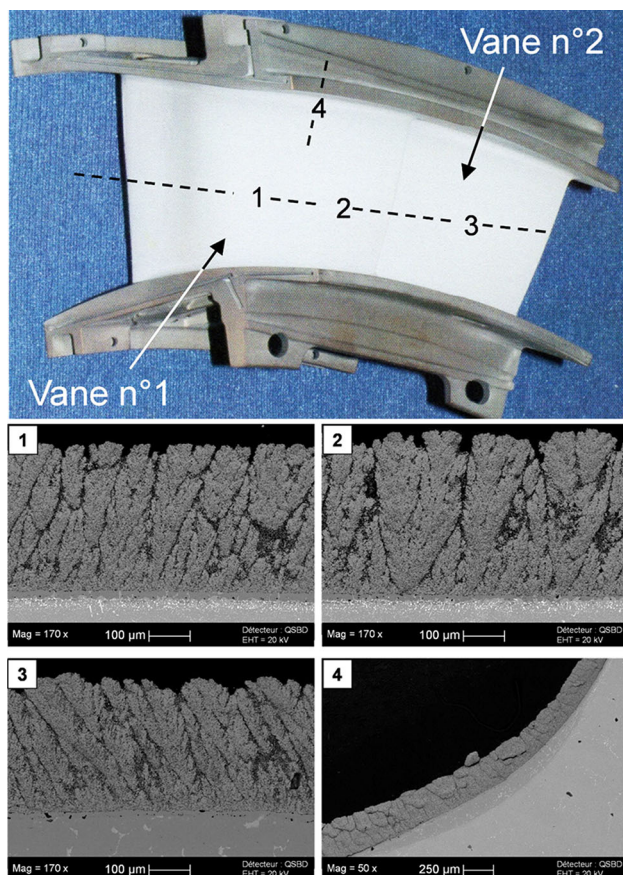


Fig. 13 High-pressure nozzle guide vane blade with an YSZ suspension plasma spray coating. SEM pictures represent the resultant microstructures at the locations pointed out on the component above

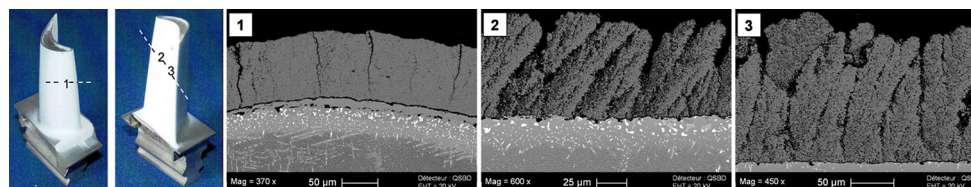


Fig. 14 High-pressure turbine blade with an YSZ suspension plasma spray coating. SEM pictures represent the resultant microstructures on the locations pointed out on the component at left

lowered in this area in order to avoid delamination or weakness which could be propagated to the vane.

For the high-pressure turbine blade, shown in Fig. 14, the SPS coating was performed on the concave side. Here, variation of spraying distances and angles are more important. Even if a columnar structure is conserved for the regions 2 and 3, the morphology and the thickness are greatly affected. For example, the coating thickness is around 150 μm in region 3 and falls to around 100 μm in region 2. For region 1, spray angle is almost off normal. In that case, deviation of particles is rather low as the plasma flow is not much deviated. A vertically cracked microstructure is obtained. Even if the morphology evolved, it could be interesting to evaluate the TCF resistance of these kinds of components. In fact, vertically cracked suspension plasma and solution precursor plasma-sprayed coatings also showed good thermal compliance (Ref 26, 32, 34).

This tends to show that for a really complex component the coating strategy and kinematic has to be adapted to keep the microstructure within the columnar range. When the SPS coating is performed on real turbine part (blade or vane for example), the spray angles and distances will not be kept constant due to the specific geometry of the component. These two parameters appeared as critical for the conservation of the microstructure. Thus, as well as for previously identified parameters (mean roughness of the substrate, the travel speed, etc.) efforts will have to be dedicated to spray angles and distances in order to ensure the conservation of columnar structure all along the profile of high-pressure turbine parts (Ref 31–33).

One of the main issues for the deposition of these kinds of components (high-pressure blades or vanes) is the conservation of airfoil cooling holes. Figure 15 shows airfoil turbine holes after SPS deposition of YSZ for the vane and the blade. In both cases, holes were conserved. The SPS coating was observed to penetrate 1 mm into the hole without any obstruction similarly to YSZ EB-PVD coatings. In the cavities, located within the component, some YSZ residues were observed. They resulted mainly from re-solidified powder or melted powder which had not enough kinetic energy to be

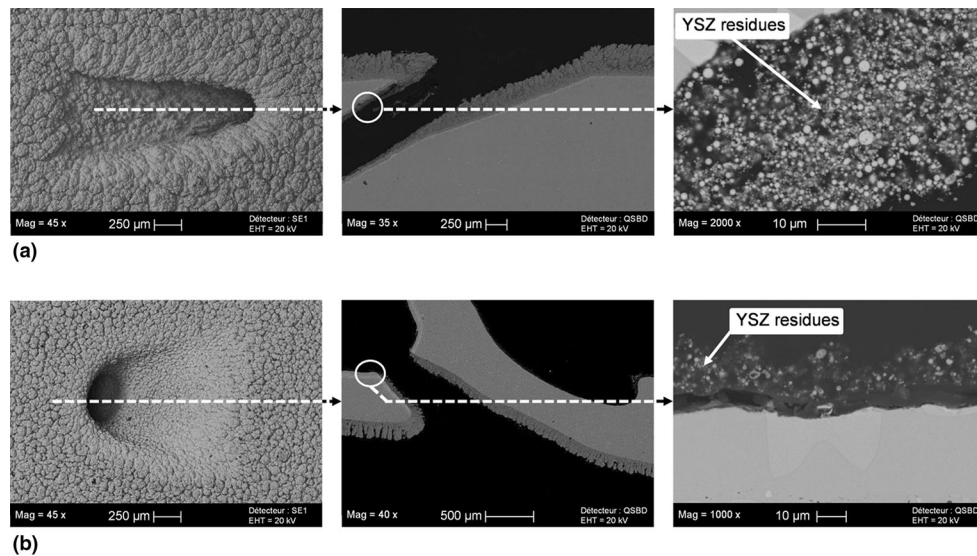


Fig. 15 SEM analysis of the airfoil cooling hole after YSZ SPS deposition of the nozzle guide vane with a hole located in region 1 of Fig. 12(a) and for the blade with a hole located in region 1 in Fig. 13(b)

spread onto the walls. These kinds of residues could be eliminated using high-pressure compressed air in the internal cooling system of components.

Conclusion

Suspension plasma spraying was used to perform and then evaluate YSZ columnar structure coatings as thermal barrier coatings. Controlling the process parameters, columnar structure was varied from a well-separated to a more compact pattern of columns.

Firstly, thermal properties of columnar YSZ coatings produced by suspension plasma spraying were acquired from room temperature to 1100 °C. Differential scanning calorimetry and flash laser techniques were applied, respectively, to determine specific heat capacity and thermal diffusivity of NiAl aluminized Hastelloy X substrate and YSZ coatings. For comparison, two optimized SPS columnar structures and a typical YSZ columnar EB-PVD were characterized. The thermal conductivity of the SPS YSZ coating was found to be lower than $1 \text{ W m}^{-1} \text{ K}^{-1}$ from room temperature up to 1100 °C irrespective of the column morphology, while the EB-PVD coating was recorded at $1.3 \text{ W m}^{-1} \text{ K}^{-1}$ at 1100 °C. These kinds of SPS columnar structures seem to be able to meet the thermal insulation requirements of the next generation of gas turbine engines.

Next, the lifetime estimated by thermal cycling fatigue tests appears promising for a TBC application irrespective of the microstructure of SPS coatings, or the bond coat used on AM1 substrate (β -(Ni,Pt)Al and platinum-diffused

γ -Ni/ γ' -Ni₃Al). However, a superior thermal cycling resistance was mainly observed for SPS columnar structure with well-separated columns compared to compact ones. The thermal compliance offered by inter-columnar voids is more efficient than vertical cracks which appeared in situ during TCF tests for the compact columnar structure.

Lifetime was found to be optimum for SPS columnar structures performed on platinum-diffused γ -Ni/ γ' -Ni₃Al bond coat presenting a low surface roughness. Indeed, the YSZ SPS columnar structure with well-separated features reached 2145 cycles to failure while 1300 cycles to failure were reached for compact ones. Results are promising with regard to the lifetime of conventional EB-PVD YSZ coatings. The higher oxidation resistance behavior of platinum-diffused γ -Ni/ γ' -Ni₃Al compared to β -(Ni,Pt)Al could explain the results.

The preparation of the bond coat surface was also a relevant parameter for the optimization of the lifetime. A high substrate roughness induced a lower organization of the YSZ SPS top coat columns leading to lower thermal compliance. For β -(Ni,Pt)Al, a preheating step of 1 h at 1100 °C prior to the YSZ coating allowed a significant increase in the thermal cycling resistance. The formation of a stable TGO prior to the deposition of top coat induced a higher resistance during TCF tests.

Failure mechanism seems linked to a sudden debonding at the TGO/substrate interface. Additional work will be carried out in order to finely describe the chronology and events which lead to the failure of the system. In the future, an effort will probably be required for the optimization of the bond coat in order to be used jointly with an YSZ columnar top coat made using SPS.

Lastly, the opportunity to coat complex turbine parts such as vanes or blades from the high-pressure parts of an aero-engine was investigated. SPS coatings presented a sufficient adhesion on the parts without debonding after spraying. Even if columnar microstructure was reached, the morphology evolved and led to vertically cracked structures at some blade locations. For example, off-normal angle during spraying was identified as relevant and needs further investigation. The turbine airfoil holes were conserved irrespective of the component.

References

- U. Schultz, B. Saruhan, K. Fritscher, and C. Leyens, Review on Advanced EB-PVD Ceramic Topcoats for TBC Applications, *Int. J. Appl. Ceram. Technol.*, 2004, **1**(4), p 302-315
- U. Schultz, C. Leyens, K. Fritscher, M. Peters, B. Saruhan-Brings, O. Lavigne, J.-M. Dorvaux, M. Poulain, R. Mévrel, and M. Caliez, Some Recent Trends in Research and Technology of Advanced Thermal Barrier Coatings, *Aerosp. Sci. Technol.*, 2003, **7**(1), p 73-80
- U. Schultz, M. Menzebach, C. Leyens, and Y.Q. Yang, Influence of Substrate Material on Oxidation Behavior and Cyclic Lifetime of EB-PVD TBC Systems, *Surf. Coat. Technol.*, 2001, **146-147**, p 117-123
- P. Fauchais, A. Vardelle, and B. Dussoubs, Quo Vadis Thermal Spraying?, *J. Therm. Spray Technol.*, 2001, **10**(1), p 44-66
- Y. Tan, V. Srinivasan, T. Nakamura, S. Sampath, P. Bertrand, and G. Bertrand, Optimizing Compliance and Thermal Conductivity of Plasma Sprayed Thermal Barrier Coatings via Controlled Powders and Processing Strategies, *J. Therm. Spray Technol.*, 2012, **21**(5), p 950-962
- N.P. Padture, M. Gell, and E.H. Jordan, Thermal Barrier Coating for Gas-Turbine Engine Applications, *Sci. Compass*, 2002, **296**, p 280-284
- R.A. Miller, Thermal Barrier Coatings for Aircraft Engines: History and Directions, *J. Therm. Spray Technol.*, 2004, **6**(1), p 35-42
- X.Q. Cao, R. Vassen, and D. Stöver, Ceramic Materials for Thermal Barrier Coatings, *J. Eur. Ceram. Soc.*, 2004, **24**(1), p 1-10
- R. Vassen, A. Stuke, and D. Stöver, Recent Development in the Field of Thermal Barrier Coatings, *J. Therm. Spray Technol.*, 2009, **18**(2), p 181-186
- R. Vassen, M.O. Jarligo, T. Steinke, D.E. Mack, and D. Stöver, Overview on Advanced Thermal Barrier Coatings, *Surf. Coat. Technol.*, 2010, **205**(4), p 938-942
- G. Suresh, G. Seenivasan, M.V. Krishnaiah, and P.S. Murti, Investigation of the Thermal Conductivity of Selected Compounds of Lanthanum, Samarium and Europium, *J. Alloys Compd.*, 1998, **269**(1-2), p L9-L12
- J. Wu, X. Wei, N.P. Padture, P.G. Klemens, M. Gell, E. Garcia, P. Miranzo, and M.I. Osendi, Low-Thermal-Conductivity Rare-Earth Zirconates for Potential Thermal-Barrier-Coating Applications, *J. Am. Ceram. Soc.*, 2002, **85**(12), p 3031-3035
- X.Q. Cao, R. Vassen, W. Jungen, S. Schwartz, F. Tietz, and D. Stöver, Thermal Stability of Lanthanum Zirconate Plasma-Sprayed Coating, *J. Am. Ceram. Soc.*, 2001, **84**(9), p 2086-2090
- R.S. Lima, A. Kucuk, and C.C. Berndt, Bimodal Distribution of Mechanical Properties on Plasma Sprayed Nanostructured Partially Stabilized Zirconia, *Mater. Sci. Eng. A*, 2002, **327**(2), p 224-232
- R.S. Lima and B.R. Marple, Nanostructured YSZ Thermal Barrier Coatings Engineered to Counteract Sintering Effect, *Mater. Sci. Eng. A*, 2008, **485**(1-2), p 182-193
- J. Wu, H.B. Guo, L. Zhou, L. Wang, and S.K. Gong, Microstructure and Thermal Properties of Plasma Sprayed Thermal Barrier Coatings from Nanostructured YSZ, *J. Therm. Spray Technol.*, 2010, **19**(6), p 1186-1194
- C. Viazzi, Elaboration par le procédé sol-gel de revêtements de zircone yttrée sur substrats métalliques pour l'application barrière thermique (Elaboration by Sol-Gel Process of Ytria Stabilized Zirconia Coatings on Metallic Substrates for Thermal Barrier Coating Application). Ph.D. thesis, University of Toulouse, France, 2007, in French
- L. Pin, F. Ansart, J.P. Bonino, Y. Le Maout, V. Vidal, and P. Lours, Reinforced Sol-Gel Thermal Barrier Coatings and Their Cyclic Oxidation Life, *J. Eur. Ceram. Soc.*, 2013, **33**(2), p 269-276
- S. Rezanika, G. Mauer, and R. Vassen, Improved Thermal Cycling Durability of Thermal Barrier Coatings Manufactured by PS-PVD, *J. Therm. Spray Technol.*, 2014, **23**(1), p 182-189
- K. Von Niessen, M. Gindrat, and A. Refke, Vapor Phase Deposition Using Plasma Spray-PVDTM, *J. Therm. Spray Technol.*, 2010, **19**(1), p 502-509
- P.L. Fauchais, J.V.R. Heberlein, and M.I. Boulos, *Thermal Spray Fundamentals from Powder to Part*, Springer, New York, 2014
- P. Fauchais, R. Etchart-Salas, V. Rat, J.F. Couderc, N. Caron, and K. Wittmann-Ténèze, Parameters Controlling Liquid Plasma Spraying: Solutions, Sols, or Suspensions, *J. Therm. Spray Technol.*, 2008, **17**(1), p 31-59
- A. Bacciochini, J. Ilavsky, G. Montavon, A. Denoirjean, F. Benettouil, S. Valette, P. Fauchais, and K. Wittmann-Ténèze, Quantification of Void Network Architectures of Suspension Plasma-Sprayed (SPS) Ytria-Stabilized Zirconia (YSZ) Coatings Using Ultrasmall-Angle X-ray Scattering (USAXS), *Mater. Sci. Eng. A*, 2010, **528**(1), p 91-102
- A. Ganvir, N. Curry, N. Markocsan, and S. Govindarajan, Characterization of Thermal Barrier Coatings Produced by Various Thermal Spray Techniques Using Solid Powder, Suspension, and Solution Precursor Feedstock Material, *Int. J. Appl. Ceram. Technol.*, 2016, **13**(2), p 324-332
- E.H. Jordan, C. Jiang, J. Roth, and M. Gell, Low Thermal Conductivity Ytria-Stabilized Zirconia Thermal Barrier Coatings Using the Solution Precursor Plasma Spray Process, *J. Therm. Spray Technol.*, 2014, **23**(5), p 849-859
- E.H. Jordan, L. Xie, M. Gell, N.P. Padture, B. Cetegen, A. Ozturk, J. Roth, T.D. Xiao, and P.E.C. Bryant, Superior Thermal Barrier Coatings Using Solution Precursor Plasma Spray, *J. Therm. Spray Technol.*, 2004, **13**(1), p 57-65
- H. Kassner, R. Siegert, D. Hathiramani, R. Vassen, and D. Stöver, Application of Suspension Plasma Spraying (SPS) for Manufacture of Ceramic Coatings, *J. Therm. Spray Technol.*, 2008, **17**(1), p 115-123
- D. Chen, E.H. Jordan, and M. Gell, Effect of Solution Concentration on Splat Formation and Coating Microstructure Using the Solution Precursor Plasma Spray Process, *Surf. Coat. Technol.*, 2008, **202**(10), p 2132-2138
- J.O. Berghaus, S. Bouaricha, J.G. Lagroux, and C. Moreau, Injection Conditions and In-Flight Particles States in Suspension Plasma Spraying of Alumina and Zirconia Nano-Ceramics, *Thermal Spray 2005: Thermal Spray Connects: Explore Its Surfacing Potential!*, E. Lugscheider, Ed., DVS-German Welding Society, Basel, 2005,
- K.J. Van Every, M.J.M. Krane, R.W. Trice, H. Wang, W. Porter, M. Besser, D. Sordelet, J. Ilavsky, and J. Almer, Column Formation in Suspension Plasma-Sprayed Coatings and Resultant

- Thermal Properties, *J. Therm. Spray Technol.*, 2011, **20**(4), p 817-828
31. P. Sokolowski, S. Kozerski, L. Pawlowski, and A. Ambroziak, The Key Process Parameters Influencing Formation of Columnar Microstructure in Suspension Plasma Sprayed Zirconia Coatings, *Surf. Coat. Technol.*, 2014, **260**, p 97-106
 32. N. Curry, Z. Tang, N. Markocsan, and P. Nylén, Influence of Bond Coat Surface Roughness on the Structure of Axial Suspension Plasma Spray Thermal Barrier Coatings—Thermal and Lifetime Performance, *Surf. Coat. Technol.*, 2015, **268**, p 15-23
 33. B. Bernard, L. Bianchi, A. Malié, A. Joulia, and B. Rémy, Columnar Suspension Plasma Sprayed Coating Microstructural Control for Thermal Barrier Coating Application, *J. Eur. Ceram. Soc.*, 2016, **36**(4), p 1081-1089
 34. N. Curry, K.J. Van Every, T. Snyder, and N. Markocsan, Thermal Conductivity Analysis and Lifetime Testing of Suspension Plasma-Sprayed Thermal Barrier Coatings, *Coatings*, 2014, **4**, p 630-650
 35. N. Curry, K. Van Every, T. Snyder, J. Susnjar, and S. Bjorklund, Performance Testing of Suspension Plasma Sprayed Thermal Barrier Coatings Produced with Varied Suspension Parameters, *Coatings*, 2015, **5**, p 338-356
 36. R. Chidambaram and S. Sampath, Characterization of the Deposition Formation Dynamics of Suspension Plasma Spray Coatings Using in situ Coating Property Measurements, in *Thermal Spray 2012: Proceedings of the International Thermal Spray Conference*, Ed., May 10-12, 2016 (Springer, Shanghai, 2016)
 37. A. Ganvir, N. Curry, N. Markocsan, P. Nylén, and F.-L. Toma, Comparative Study of Suspension Plasma Sprayed and Suspension High Velocity Oxy-Fuel Sprayed YSZ Thermal Barrier Coatings, *Surf. Coat. Technol.*, 2015, **268**, p 70-76
 38. B. Bernard, A. Quet, L. Bianchi, A. Joulia, A. Malié, V. Schick, and B. Rémy, Thermal Insulation Properties of YSZ Coatings: Suspension Plasma Spraying (SPS) Versus Electron Beam Physical Vapor Deposition (EB-PVD) and Atmospheric Plasma Spraying (APS), *Surf. Coat. Technol.*, 2017, **318**, p 122-128
 39. Z. Tang, H. Kim, I. Yaroslavski, G. Masindo, Z. Celler, and D. Ellsworth, Novel thermal barrier coatings produced by axial suspension plasma spray, in *Thermal Spray 2011: Proceedings of the International Thermal Spray Conference*, ed. by B.R. Marple, A. Agarwal, M.M. Hyland, Y.-C. Lau, C.-J. Li, R.S. Lima, and A. McDonald, September 27-29, 2011 (Springer, Hamburg, 2012), p. 372
 40. F.-R. De Hoog, J.-H. Knight, and A.-N. Stokes, An Improved Method for Numerical Inversion of Laplace Transforms, *SIAM J. Sci. Stat. Comput.*, 1982, **3**(3), p 357-366
 41. K. Levenberg, A Method for the Solution of Certain Nonlinear Problems in Least Squares, *Quart. J. Appl. Math.*, 1944, **2**(2), p 164-168
 42. D.W. Marquardt, An Algorithm for Least-Squares Estimation of Nonlinear Parameters, *J. Soc. Ind. Appl. Math.*, 1963, **11**(2), p 68-78
 43. B. Rémy, S. André, and D. Maillat, Non Linear Parameter Estimation Problems: Tools for Enhancing Metrological Objectives, *Eurotherm Adv. Mett 5 Spring Sch.*, 2011, **4**, p 1-71
 44. J. Eldridge and C. Spuckler, Determination of Scattering and Absorption Coefficients For Plasma-Sprayed Yttria-Stabilized Zirconia Thermal Barrier Coatings, *J. Am. Ceram. Soc.*, 2008, **91**(5), p 1603-1611
 45. J. Eldridge, C. Spuckler, and R. Markham, Determination of Scattering and Absorption Coefficients for Plasma-Sprayed Yttria-Stabilized Zirconia Thermal Barrier Coatings at Elevated Temperatures, *J. Am. Ceram. Soc.*, 2009, **92**(10), p 2276-2285
 46. V.K. Tolpygo and D.R. Clarke, The Effect of Oxidation Pretreatment on the Cyclic Life of EB-PVD Thermal Barrier Coatings with Platinum–Aluminide Bond Coats, *Surf. Coat. Technol.*, 2005, **200**(5-6), p 1276-1281
 47. V. Deodeshmukh, N. Mu, B. Li, and B. Gleeson, Hot Corrosion and Oxidation Behavior of a Novel Pt + Hf-Modified γ' -Ni₃Al + γ -Ni-Based Coating, *Surf. Coat. Technol.*, 2006, **201**(7), p 3836-3840
 48. T. Izumi, N. Mu, L. Zhang, and B. Gleeson, Effect of Targeted γ -Ni + γ' -Ni₃Al-Based Coating Compositions on Oxidation Behavior, *Surf. Coat. Technol.*, 2007, **202**(4-7), p 628-631
 49. J.A. Haynes, B.A. Pint, Y. Zhang, and I.G. Wright, Comparison of the Cyclic Oxidation Behavior of β -NiAl, β -NiPtAl and γ - γ' NiPtAl Coating on Various Superalloys, *Surf. Coat. Technol.*, 2007, **202**(4-7), p 730-734
 50. P.K. Wright and A.G. Evans, Mechanisms Governing the Performance of Thermal Barrier Coatings, *Curr. Opin. Solid State Mater. Sci.*, 1999, **4**(3), p 255-265
 51. A.G. Evans, D.R. Clarke, and C.G. Levi, The Influence of Oxides on the Performance of Advanced Gas Turbines, *J. Eur. Ceram. Soc.*, 2008, **28**(7), p 1405-1419